High-Frequency Magnetoacoustic Measurements in Indium and Lead

JOHN A. RAYNE
Westinghouse Research Laboratories, Pittsburgh, Pennsylvania
(Received 20 August 1962)

Magnetoacoustic measurements at frequencies up to 270 Mc/sec have been made on high-purity indium and lead single crystals. Automatic data recording was employed, the attenuation being obtained directly as a function of $1/H$. Well-defined periodic behavior was observed for both metals, enabling accurate extremal dimensions of the respective Fermi surfaces to be obtained. The results agree reasonably well with the predictions of the free-electron model.

I. INTRODUCTION

MAGNETOACOUSTIC data on indium[1,2] and lead[3] have previously been reported. In neither metal, however, is the reported oscillatory behavior sufficiently well defined to enable accurate extremal dimensions of the Fermi surface to be deduced. For this reason, further magnetoacoustic measurements have been made at frequencies up to 270 Mc/sec on high-purity samples. Automatic recording has been employed, the attenuation being obtained directly as a function of $1/H$. The resulting oscillatory behavior is very pronounced and, in general, gives very accurate extremal dimensions of the Fermi surface. Fair agreement is obtained with the values predicted from the free-electron model. For the case of lead, the data are in extremely good agreement with the results of the OPW interpolation scheme of Anderson.[4]

II. EXPERIMENTAL

Measurements were made at frequencies up to 270 Mc/sec using the experimental setup shown in Fig. 1. 1-μsec rf pulses of approximately 100-V amplitude are produced in a tuned line oscillator employing a 6939 twin pentode. Screen grid modulation is used. The attenuation is measured by a transmission method, both the transmitting and receiving transducers being 30-Mc/sec X-cut crystals excited at an odd harmonic.

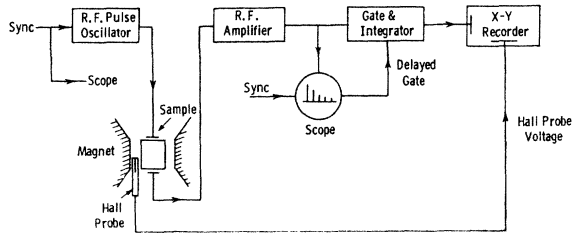

FIG. 1. Schematic diagram of experimental arrangement for high-frequency magnetoacoustic measurements.

After amplification the received pulses pass to a gated amplifier, which is actuated by a pulse derived from the delay circuit of a 545 Tektronix oscilloscope. The amplitude of the selected pulse is then measured by means of a diode integrating circuit and is displayed on the Y axis of a Moseley type 2D-2 recorder. A Bell Model 120 gaussmeter measures the magnetic field. The resulting voltage is applied to the modified X amplifier of the recorder, so as to give a deflection which is proportional to $1/H$. By sweeping the magnetic field, a plot of received signal amplitude as a function of $1/H$ is thus automatically obtained. Figure 2 shows a typical curve obtained for indium at a frequency of 210 Mc/sec using longitudinal waves.

Considerable care was exercised in the preparation of the single crystals used in these experiments. Single-crystal ingots of both indium and lead were produced by the Bridgman technique. These ingots were oriented by x rays and suitable acoustic specimens cut from them by a Servomet spark erosion apparatus. In all cases, it was found necessary to plane the faces of the specimens to be flat and parallel within 0.0001 in., so as to obtain good echoes through the sample. No mechanical lapping was used, because the polycrystalline recrystallized layer produced by this procedure caused excessive scattering of the high-frequency sound waves. The sample length varied from 2 to 4 mm.

All the present data were taken using longitudinal

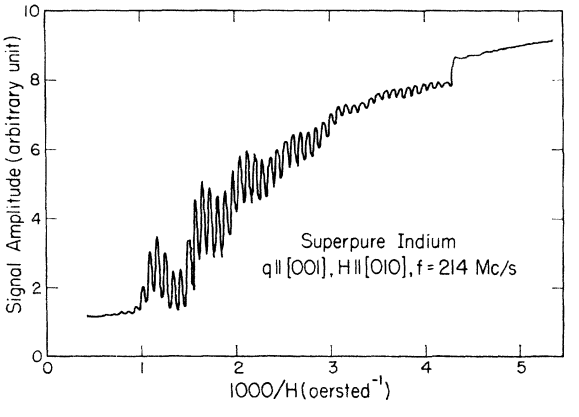

FIG. 2. Typical recorder tracing obtained for indium at 210 Mc/sec using longitudinal waves. The propagation direction is [001] and the temperature is approximately 1.3°K.

[1] A. A. Galkin, E. A. Kaner, and A. P. Korolyuk, J. Exptl. Theoret. Phys. (U.S.S.R.) **39**, 1517 (1960).
[2] J. A. Rayne and B. S. Chandrasekhar, Phys. Rev. **125**, 1952 (1962).
[3] A. R. Macintosh, *The Fermi Surface* (John Wiley & Sons, Inc., New York, 1960), p. 233; Proc. Roy. Soc. (London) (to be published).
[4] J. R. Anderson, Ph.D. thesis, Iowa State University, 1962 (unpublished).

waves, the specimen temperature being approximately 1.3°K so as to obtain a long electron mean-free path unaffected by phonon scattering. For indium, some data were obtained at 270 Mc/sec, but it was found that essentially the same information could be obtained with greater ease at 150 Mc/sec. The discontinuity in the signal amplitude at $H\sim240$ G corresponds to the transition from the normal to the superconducting state. Measurements were made with $q\|[010]$, [110], [001], and (111) at angular intervals of H never in excess of five degrees. For lead, all data were obtained at 270 Mc/sec with $q\|[100]$, [110], and [111], respectively.

III. RESULTS

Representative tracings of the data taken on indium are shown in Fig. 3. In all cases at least one prominent period with no fewer than 20 oscillations was observed, thus enabling very accurate extremal wave numbers to be obtained from the formula

$$k_{\text{ext}}=(e/2\hbar c)[\lambda/\Delta(1/H)]. \quad (1)$$

Here λ is the sound wavelength appropriate to the propagation vector $\mathbf{q}$ and $\Delta(1/H)$ the corresponding period of the oscillation. It is assumed that k_{ext} is the extremal value of the wave number vector for the Fermi surface in the direction $\mathbf{q}\times\mathbf{H}$. As discussed by Pippard,[5] this assumption may not necessarily be correct; the main justification in the present instance is that it gives results which seem to be eminently reasonable. Figure 4 shows the angular variation of

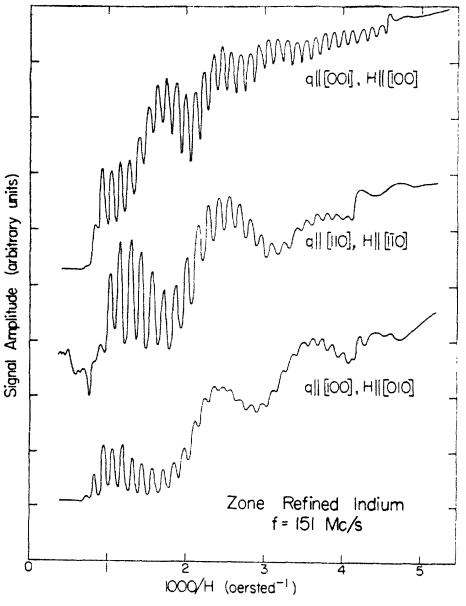

FIG. 3. Representative tracings of data obtained on indium using longitudinal waves at 150 Mc/sec.

[5] A. B. Pippard, Proc. Roy. Soc. (London) **A257**, 165 (1960).

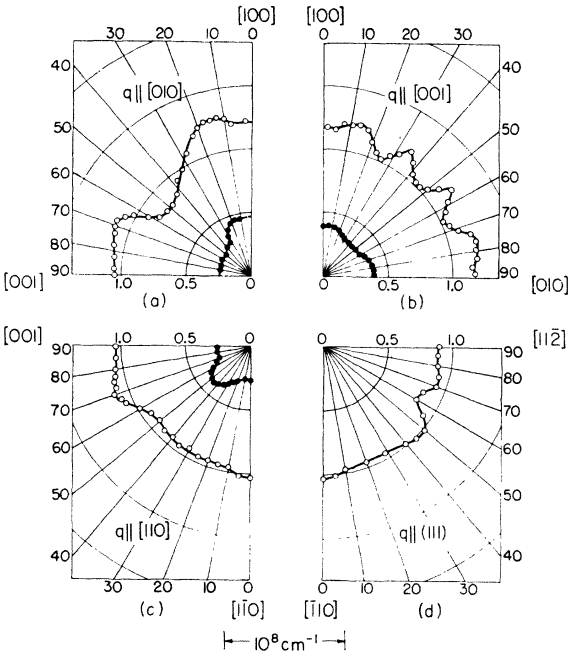

FIG. 4. Angular variation of k_{ext} for indium computed from Eq. (1). It should be noted that the smaller dimensions are extremal diameters.

k_{ext} computed from Eq. (1). Except for $q\|(111)$, both long- and short-period oscillations are observable; it should be noted that in Fig. 4 the values of k_{ext} for the long-period oscillations are extremal diameters.

Typical data for lead are shown in Figs. 5 and 6. In this case the critical field is approximately 800 Oe, so that many of the low-field oscillations are no longer

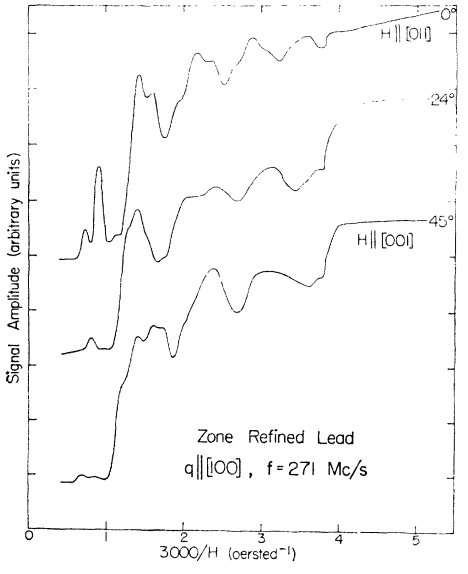

FIG. 5. Representative data obtained for lead using longitudinal waves at 270 Mc/sec. The propagation direction is [100] and the temperature is approximately 1.3°K.

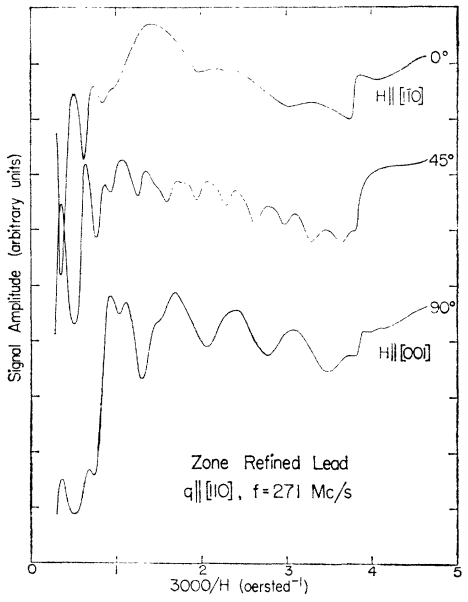

FIG. 6. Representative data obtained for lead using longitudinal waves at 270 Mc/sec. The propagation direction is [110] and the temperature is approximately 1.3°K.

visible due to the onset of superconductivity. It was thus necessary to use as high a frequency as possible for all measurements. Even at 270 Mc/sec, however, relatively few short-period oscillations are observed for most field orientations. This is presumably due to orbit interference effects, whose existence has previously been postulated by Mackintosh.[3] Figure 7 shows the extremal dimensions of the wave number vector for lead with $q\|[100]$ and $q\|[110]$, using the sound wavelength λ computed from the elastic constants of Alers and Waldorf.[6] Because of the restricted number of oscillations, particularly for the short-period data, the scatter is much larger than in the case of indium. In all cases, the discontinuous change in signal amplitude for low fields corresponds to the transition from the normal to the superconducting state.

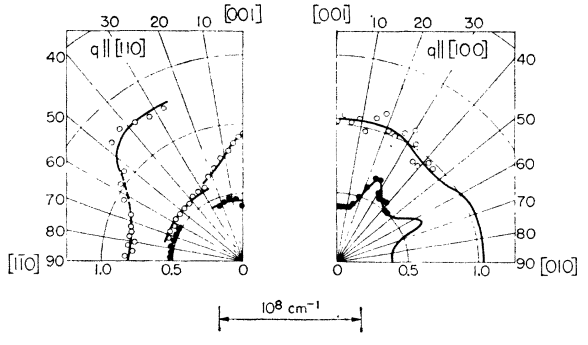

FIG. 7. Angular variation of k_{ext} for lead computed from Eq. (1). It should be noted that the third zone dimensions in solid circles are extremal diameters (see Fig. 11).

[6] D. L. Waldorf, Bull. Am. Phys. Soc. 5, 170 (1959).

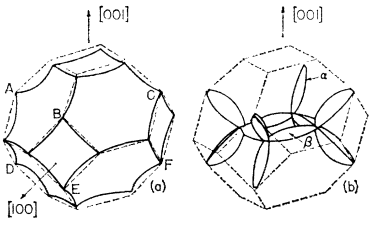

FIG. 8. Free-electron Fermi surface for indium; small pockets of electrons in the fourth zone are not shown.

IV. DISCUSSION

A. Indium

The free-electron Fermi surface for indium is shown in Fig. 8. The first zone is full, while the second is a dimpled fourteen-sided polyhedron similar to that in aluminum. Owing to the tetragonal structure of indium, which has $c/a=1.08$, the square faces perpendicular to [001] are larger than those parallel to [001]. A similar distortion exists in the arms α, β of the third zone. Relevant cross sections of the second and third zone surfaces are shown in Fig. 9; the lettered dimensions will subsequently be compared to the experimental values. As discussed in a previous paper, the second zone on the free-electron model is multiply connected at the points A, B, C, D, E, F, etc. This feature does not appear to be supported by magnetoresistance data.[7] Small pockets of electrons are predicted in the fourth zone but these presumably disappear in a finite crystal potential.

The larger extremal dimensions of Fig. 4 undoubtedly are associated with the second zone surface for indium. Comparison with the cross sections of Fig. 9 shows the

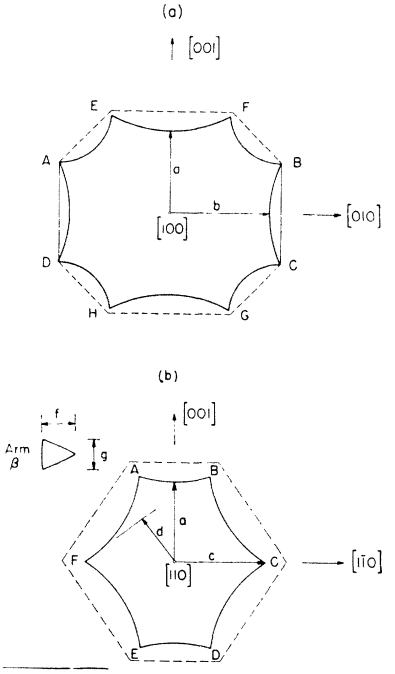

FIG. 9. Cross sections of the second and third zones for indium according to the free-electron model.

[7] N. E. Alekseevskii and Yu. P. Gaidukov, J. Exptl. Theoret. Phys. (U.S.S.R.) 37, 672 (1959).

TABLE I. Comparison of extremal dimensions of Fermi surface for indium with free-electron model.

Zone	Dimension designation	Theoretical dimension[a]	Experimental dimension	Mean Expt'l[b]
2	a	1.04	1.03(1) 1.03(3)	1.03
	b	1.24	1.21(1) 1.17(2)	1.19
	c	1.13	1.03(2) 1.03(3) 1.03(4)	1.03
3	d	0.69	0.95(3)	0.95
	f	0.42	0.35(2)	0.35
	g	0.39	0.25(3)	0.25

[a] All in units of 10^8 cm^{-1}.
[b] Crystals with $q\|$ [010], [001], [110], and (111) designated as 1, 2, 3, and 4, respectively.

existence of a surprising degree of correspondence between the two. As would be expected, the cusps of the free-electron model are not reproduced, but there seems to be little doubt as to the essential correctness of the topology of the free-electron model for indium. Along axes of high symmetry, there is no question that the extremal dimensions measured do, in fact, correspond to the actual dimensions of the Fermi surface in these directions. Table I shows a comparison between the theoretical values and those obtained from experiment. For the dimensions a, b, the agreement is within experimental error. The dimension c, however, is smaller than that obtained from theory, again suggesting a rounding of the cusps associated with the free-electron model. Both Figs. 4(c) and 4(d) suggest that the dimpled hexagonal faces are pulled out towards ⟨111⟩ directions and that, in fact, they are almost spherical about the immediate vicinity of these directions. The angular extensions of the "square" faces perpendicular and parallel to [001] are about 23° and 15°, respectively, compared to the theoretical values of 30° and 25°. As before, this disagreement is easily explained in terms of the absence of the cusp-like geometry inherent in the free-electron model. No evidence has been obtained for the existence of oscillations associated with orbits around the necks of the second zone surface.

It is believed that the smaller extremal dimensions of Fig. 4 are associated with the third zone surface for indium. Reference to Table I shows that the agreement with the free-electron model is also quite good. As may be seen from Fig. 4(b), the extremum increases from [110] to [010]. However, the change is small, which would be expected if the arms were tapered rather than

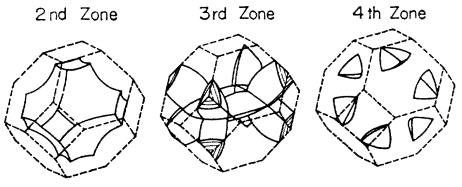

FIG. 10. Free-electron Fermi surface for lead.

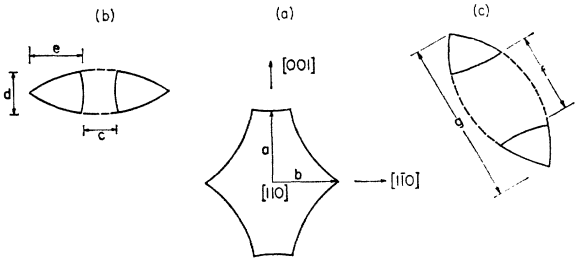

FIG. 11. Cross sections of the second and third zone surfaces for lead according to the free-electron model.

cylindrical. This viewpoint finds additional support from the curve Fig. 4(c); for an arm of cylindrical cross section, the extremal dimension would increase continuously as H is rotated away from [110]. In summary, then, it would seem that the free-electron model does provide a quite accurate model for the Fermi surface of indium.

B. Lead

Figure 10 shows the free-electron Fermi surface for lead.[8] The first zone is full while the second zone surface is a dimpled fourteen-sided polyhedron, the faces of which are smaller than those for a trivalent fcc metal. Correspondingly, the third zone arms are much thicker than in the latter case. Small pockets of electrons also are predicted to exist in the fourth zone, but recent de Haas–van Alphen data[9] have failed to confirm their existence. Thus, we can presumably confine our attention to orbits in the second and third zones. The relevant cross sections of the Fermi surface are shown in Fig. 11. Owing to the thicker arms existing in the third zone, the associated oscillatory effects are quite pronounced. Figure 12 shows the possible orbits on a

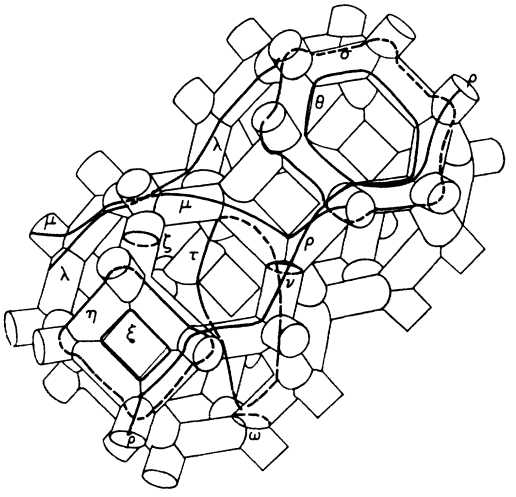

FIG. 12. Schematic representation of the possible third zone orbits in lead.

[8] Walter A. Harrison, Phys. Rev. 118, 1182 (1961).
[9] A. V. Gold and J. R. Anderson (private communication).

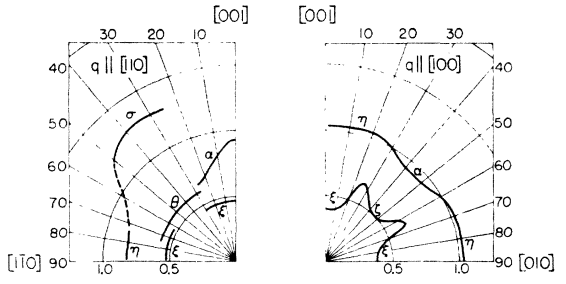

FIG. 13. Tentative assignment of the observed extrema to the possible orbits in lead. *Note added in proof.* For $\mathbf{q}\|[110]$, $\mathbf{H}\sim[1\bar{1}0]$ the smaller extremum corresponds to the orbit ζ not ξ.

schematic representation of the third zone. As noted previously, there are many field orientations for which orbits are simultaneously present on the second and third zone surfaces. It is believed that the interference effects between such orbits is responsible for the relatively few oscillations observed for many field orientations.

Reference to Fig. 7 shows that, in general, two distinct momenta are observed for any direction of the magnetic field. On the basis of the free-electron model, it is possible to make an identification of the associated orbits; a tentative scheme is given in Fig. 13. The most certain assignment concerns the oscillations associated with the orbit θ. These occur for $\mathbf{q}\|[110]$, $\mathbf{H}\sim[1\bar{1}1]$, a typical curve for $\mathbf{H}$ at 45° to [001] being shown in Fig. 6. There is fair agreement between the angular range over which these oscillations can be observed and that predicted from the free-electron model, modified so as to round off the cusps of the resulting surface. As may be seen from Table II, the extremal dimension agrees quite closely with the calculated value. It would thus seem natural to assign the larger extremal dimensions for $\mathbf{q}\|[110]$, $\mathbf{H}\sim[1\bar{1}1]$ to the orbits σ, which involve the outer parts of the hexagonal surfaces of the third zone. From Table II, it is seen that this assignment again gives an extremal dimension in fairly good agreement with experiment.

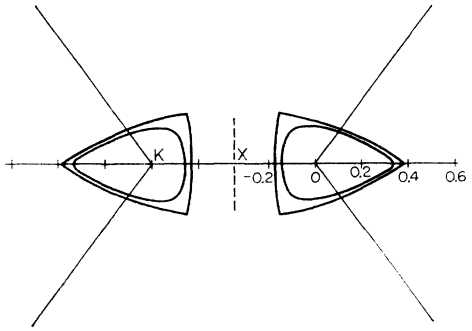

FIG. 14. Section of the third zone surface for lead according to the free-electron model and the OPW interpolation scheme of Anderson.[4] The projection is along [110] and the dimensions are in units of $2\pi/a$.

For $\mathbf{q}\|[100]$, $\mathbf{H}\sim[001]$ orbits involving both the second and third zones are possible. The former involve relatively limited extremal regions, since they transverse the cusp-like ridges of the second zone. It would therefore seem to be more reasonable that the oscillatory behavior with $\mathbf{H}$ near [001] is due to the orbit η. For $\mathbf{H}$ near [011], however, it seems fairly certain that a second zone orbit predominates. This orbit encompasses both the square and hexagonal faces of the second zone; it thus would be expected to possess a large area giving extrema. For the same reason it would appear that the oscillatory behavior for $\mathbf{q}\|[110]$, $\mathbf{H}\sim[1\bar{1}0]$ is also due to the orbits α. Reference to Table II shows that these assignments give dimensions agreeing quite closely with each other and with the value predicted from the free-electron model. Using this same argument, it seems reasonable to assign the oscillations for $\mathbf{q}\|[110]$, $\mathbf{H}\sim[001]$ to the third zone orbits η. The third zone orbits ξ, ζ are undoubtedly responsible for the long-period oscillations observed.

TABLE II. Comparison of extremal dimensions of Fermi surface for lead with theoretical values.

Zone	Dimension designation	Theoretical[a] dimension: Free electron	Theoretical[a] dimension: OPW	Experimental dimension[b]	Mean[a] expt'l.
2α	a	0.98	0.95	0.92(2)	0.92
2α	b	0.87	0.85	0.92(1)	0.92
3ξ	Diagonal	0.67	0.67	0.40(1)	0.40
3ξ	c	0.44	0.52	0.52(2)	0.52
3η	Semidiagonal	0.93	0.86	1.03(1)	1.03
3η	$e+\frac{1}{2}c$	0.93	0.84	0.83(2)	0.83
3ζ	d	0.59	0.42	0.50(1) 0.45(2)	0.48
3θ	$\frac{1}{2}f$	0.55	0.56	0.58(2)	0.58
3σ	$\frac{1}{2}g$	1.12	0.99	1.28(2)	1.28

[a] All in units of 10^8 cm^{-1}.
[b] Crystals with $q\|$ [100] and [110] designated as 1 and 2, respectively.

From Table II it may be seen that, in general, the extermal dimensions agree quite well with those obtained from the free-electron model. This result is consistent with the recent work of Gold and Anderson,[9] who find that the high-field de Haas–van Alphen data on lead are also in reasonable agreement with the free-electron model if the fourth zone pockets are removed. It has been shown by Anderson, however, that an even better fit with experiment can be obtained using an OPW interpolation procedure. This scheme modifies the cross sections of the free-electron Fermi surface mainly by rounding off the cusps inherent in the latter, as may be seen in Fig. 14. In Table II a comparison is also given with the extremal dimensions given by this model; the agreement is clearly very good and, in fact, appears to be within the limits of error of the magnetoacoustic data. It must be concluded that the OPW model is extremely satisfactory at least insofar as the present data are concerned.

V. CONCLUSIONS

High-frequency magnetoacoustic data have been obtained for both indium and lead using an automatic recording technique. For both metals reasonable agreement is obtained between the extremal dimensions of the Fermi surface and those obtained from the free-electron model. The OPW model of Anderson gives an even better fit to the data for lead.

ACKNOWLEDGMENTS

The author would like to thank P. Hodder who grew the lead crystals used in these experiments. Thanks are also due to Dr. A. V. Gold and Dr. J. R. Anderson for several helpful discussions. Special thanks are due to Dr. A. R. Mackintosh for many enlightening suggestions and for providing a copy of his paper prior to publication.

PHYSICAL REVIEW VOLUME 129, NUMBER 2 15 JANUARY 1963

Theory of the Intrinsic Electronic Thermal Conductivity of Superconductors*

LUDWIG TEWORDT
Department of Physics, University of Notre Dame, Notre Dame, Indiana
(Received 27 August 1962)

The analog to the Bloch equation for the case of thermal conduction in a superconductor limited by phonon scattering is derived by introducing an appropriate general form for the nonequilibrium part of the distribution function into the corresponding Boltzmann equation. This integral equation for the deviation function is solved numerically for different temperatures T by replacing it by sets of simultaneous linear equations with dimensions up to 39. The limiting curve for the deviation function when T approaches the transition temperature T_c from below turns out to be identical to the curve which has been reported by Klemens for the normal state. With T decreasing below T_c the maximum of the deviation function rises and shifts to higher energies. The ratio of the thermal conductivity in the superconducting state to that in the normal state, κ_s/κ_n, plotted against T/T_c is found to increase monotonically and to have a limiting slope of about 1.62 at T_c. Consideration of the energy dependence of the energy gap in the case of lead yields a sizable effect on the plot of κ_s/κ_n vs T/T_c.

I. INTRODUCTION

AN outstanding feature of the experimental results for the electronic thermal conductivity of superconductors is the qualitatively different behavior of the conductivity according to whether the dominant scatterers are impurities or phonons. The ratio of the thermal conductivity in the superconducting state to that in the normal state, κ_s/κ_n, plotted against the reduced temperature, T/T_c, is found to have a zero slope at the transition temperature T_c if the scattering is predominantly by the impurities, but it is found to have a finite limiting slope, of about 1.6 for tin and of about 5 for lead and mercury, if the scattering is predominantly by phonons.

Bardeen, Rickayzen, and the author[1] have derived an expression for κ_s/κ_n on the basis of the Bardeen-Cooper-Schrieffer microscopic theory of superconductivity,[2] valid when the impurity scattering limits the heat flux. They find excellent agreement between their theoretical curve and the various experimental data; in particular, this theory yields a zero slope of κ_s/κ_n at T_c. So far, the electronic thermal conductivity limited by the phonons has not been understood as well. This problem has been treated first in BRT by setting up the full Boltzmann equation for the deviation in the distribution function of the quasi-particles from the equilibrium distribution. This Boltzmann equation takes into account the occurrence of the energy gap in a superconductor, the modified group velocity of the quasi-particle excitations, and the coherence factors in the matrix elements for the particle-phonon interaction. Lower bounds on the thermal conductivity were obtained by making use of Kohler's variational principle. One of the trial solutions which were used for the deviation function gave a negative slope of κ_s/κ_n versus T/T_c at T_c.

Kadanoff and Martin[3] derived an approximate expression for κ_s/κ_n by using thermodynamic Green's functions and introducing a finite lifetime for the excitations as a parameter into the theory. Their basic approximation consists in the replacement of the transport cross section by the scattering cross section. In evaluating their expression for κ_s/κ_n they further assumed that the lifetimes of a quasi-particle and a normal state excitation are the same and do not depend on the excitation energy. Under these assumptions the two (unknown) lifetimes drop out from the expression for κ_s/κ_n, and the temperature dependence of this ratio

* This work was supported in part by the National Science Foundation.

[1] J. Bardeen, G. Rickayzen, and L. Tewordt, Phys. Rev. **113**, 982 (1959), hereafter referred to as BRT.

[2] J. Bardeen, L. N. Cooper, and J. R. Schrieffer, Phys. Rev. **108**, 1175 (1957), hereafter referred to as BCS.

[3] L. P. Kadanoff and P. Martin, Phys. Rev. **124**, 670 (1961).